Ultrafast Science
A SCIENCE PARTNER JOURNAL

RESEARCH ARTICLE

Coherent Terahertz Wave Generation from Mono- and Multilayer MoS_2 through Quantum Interference

Yuhang He, Yuxuan Chen, Xiangyu La, Chenyin Dai, Zhen Tian*, and Jianming Dai*

Center for Terahertz Waves and School of Precision Instrument & Opto-electronics Engineering, Tianjin University, Tianjin 300072, China.

*Address correspondence to: jianmingdai@tju.edu.cn (J.D.); tianzhen@tju.edu.cn (Z.T.)

Citation: He Y, Chen Y, La X, Dai C, Tian Z, Dai J. Coherent Terahertz Wave Generation from Mono- and Multilayer MoS_2 through Quantum Interference. *Ultrafast Sci.* 2024;4:Article 0069. https://doi.org/10.34133/ultrafastscience.0069

Submitted 1 March 2024
Accepted 17 June 2024
Published 23 August 2024

Quantum interference (QI) has been widely studied in advanced materials and can be exploited to control the nonlinear response by varying the relative phase between the incident optical pulses. However, the contribution of the coherent injected photocurrent by QI from the indirect gap materials is still unclear because of the much weaker phonon-assisted absorption compared with that from the direct gap materials. Here, we investigate the coherent injected photocurrent in mono- and multilayer MoS_2 with thickness at the nanometer scale under 2-color light excitation by detecting the generated coherent terahertz (THz) wave. We observe that the THz radiation can be controlled by the relative phase. Besides, we obtain similar experimental results of the THz wave generation from mono- and multilayer MoS_2 when we change the relative polarization angle between ω and 2ω pulses, in comparison to the case of direct gap materials. Thus, these experimental results further verify that, in multilayer MoS_2 with an indirect gap, QI in the direct gap region is the dominant process for the THz wave generation. Furthermore, we demonstrate that QI can be a more effective mechanism to induce THz radiation than optical rectification under single-color light excitation. This study enhances the understanding of QI in indirect gap materials and highlights the potential of 2-color light excitation for investigating third-order nonlinear processes in advanced materials.

Introduction

Terahertz (THz) wave generation from advanced materials under pulsed light excitation is an alternative approach to explore the native nonlinearities of materials [1–3]. The revealed nonlinearities from THz wave generation have attracted great interest for fundamental research and disruptive applications in imaging [4–6], spectroscopy [7,8], and the design of optoelectronic devices [9,10]. As one of the main methods, second-order nonlinear processes, such as optical rectification (OR) [11,12], photo drag effect [13,14], and photovoltaic effect [15,16], have been utilized to induce the THz wave generation from materials by using a single-color light excitation. Nevertheless, such second-order nonlinear processes are limited by their requirement of symmetry breaking [17]. As an alternative method, the 2-color light excitation has been utilized to study the third-order nonlinearities in both centrosymmetric and noncentrosymmetric materials [18,19]. Two-color light excitation method is widely used to generate THz radiation from traditional bulk semiconductor materials [20,21], as well as laser-induced plasma in gaseous and liquid materials [22–24]. Recently, this method has been extended to investigate the nonlinearities in 2D materials and quasi-2D surface, such as graphene [25,26] and air–InAs interface [27]. The mechanism for THz wave generation from these materials is attributed to the quantum interference (QI) under 2-color light excitation [19,28].

QI can be induced by the interference between the 2 transition pathways that connect the same initial and final states in the valence and conduction bands. In general, the 2 transition pathways in the material are clarified as 2-photon absorption (TPA) and single-photon absorption (SPA) of fundamental and second-harmonic pulses, respectively. When the bandgap of the material E_g lies between the photon energies of the fundamental light $\hbar\omega$ and the second harmonic $2\hbar\omega$, i.e., $\hbar\omega < E_g < 2\hbar\omega$ [29,30], an asymmetric carrier distribution in the conduction band (CB) can be induced by QI, resulting in coherent injected photocurrent. Besides, the coherent injected photocurrent can be detected experimentally by monitoring the THz radiation emitted from materials [31]. In particular, the most crucial application of QI under 2-color light excitation is coherent control. The direction and amplitude of the injected photocurrent can be coherently controlled by the relative phase between the ω and 2ω pulses [32,33]. This concept has been applied to coherently control the photoionization of atoms [34], as well as photocurrents in semiconductors and graphene [25,29]. Nevertheless, most of the controllable coherent injected photocurrent studies mainly focus on direct bandgap materials, such as GaAs [20], ZnTe [35], and Bi_2S_3 [36]. The coherent injected photocurrent generated from QI in the indirect gap region has seldom been considered due to the weak optical response. Previous investigations have demonstrated the coherent injected photocurrent from QI in different materials with

only direct or indirect gap [18,37]. However, there is still a lack of investigations focusing on QI in the same kind of materials with both direct and indirect gaps. Therefore, it is important to present a clear view of QI in the same materials with both direct and indirect gaps under 2-color light excitation.

Recently, transition metal dichalcogenide (TMD) materials, as one of the typical 2-dimensional (2D) materials, have attracted much attention due to their excellent linear and nonlinear properties [38,39]. Molybdenum disulfide (MoS_2), as an emerging 2D layered TMDs material, possesses extraordinary physical, electrical, and optical properties. Multilayer MoS_2 has indirect gap in its band structure, while monolayer MoS_2 has direct bandgap [40–42]. Therefore, MoS_2 is an attractive candidate for various photonic and optoelectronic applications, such as phototransistors [43], photodetectors [44,45], and heterojunction solar cells [46]. Moreover, the inter- and intra-band nonlinearities are abundant in MoS_2 due to its adjustable electric band structure [47,48]. Thus, MoS_2 material with direct and indirect gaps can be expected as a platform for investigating QI-induced coherent injected photocurrent. While THz wave generation (i.e., photocurrent) from bulk MoS_2 has been demonstrated through a second-order nonlinear process under single-color light excitation [49,50], relevant research on the generation of THz wave under 2-color laser excitation is still absent.

In this letter, we employ a 2-color light excitation method to examine the coherent injected photocurrent in MoS_2 materials by monitoring the THz radiation emitted from both monolayer and multilayer MoS_2. Notably, we have successfully detected THz radiation from the atomic layer of MoS_2, and stronger THz radiation can be observed from multilayer MoS_2. By changing the relative phase between the ω and 2ω pulses, we demonstrate that the polarity and amplitude of the coherent THz wave generated from MoS_2 can be controlled. These experimental results provide experimental evidence that the mechanism of THz wave generation from MoS_2 can be attributed to QI. Moreover, the dependence of THz waves on the relative polarization angle between the ω and 2ω pulses is similar for both mono- and multilayer MoS_2. Thus, the mechanism of THz wave generation from multilayer MoS_2 can be explained by QI in the direct gap region. To compare QI and OR, we measure the THz radiation from multilayer MoS_2 under 2-color light excitation at oblique incidence condition and QI is more efficient than OR in THz wave generation from MoS_2. Therefore, this work not only explores QI in materials with both direct and indirect gaps but also contributes to the fundamental research of MoS_2 materials in the field of nonlinear optics.

Materials and Methods

In the experiment, the MoS_2 materials are grown on z-cut sapphire substrates by chemical vapor deposition (Sixcarbon Tech Shenzhen). Figure 1A shows the Raman spectra of the mono- and multilayer MoS_2. Peaks at 383.5 and 404.8 cm^{-1} (~380.6 and 407.6 cm^{-1}) in Fig. 1A are typical Raman modes of the monolayer (or multilayer) MoS_2 and indicate the in-plane E_{2g}^1 and the out-of-plane A_{1g} modes, respectively [51]. The peak at 417.2 cm^{-1} is associated with the sapphire substrate [52]. To confirm the thickness of the mono- and multilayer MoS_2, we measure the thickness of the mono- and multilayer MoS_2 samples using atomic force microscope (AFM) as shown in Figs. 1B and C. The thickness of the monolayer MoS_2 is about 0.8 nm, which agrees with the thickness for S-Mo-S atomic structures [53]. We can also obtain that the thickness of the multilayer MoS_2 is about

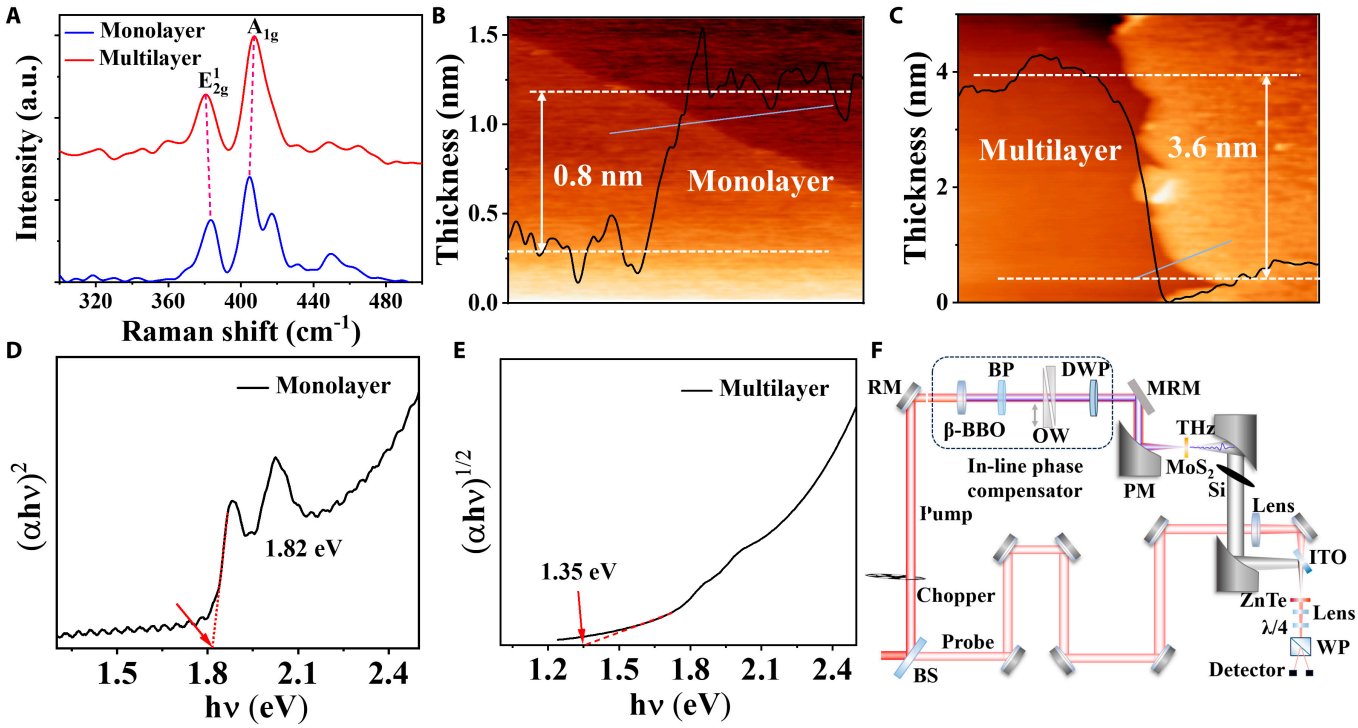

Fig. 1. (A) Raman spectra of the mono- and multilayer MoS_2. (B and C) AFM images of the mono- and multilayer MoS_2, respectively. Black lines show the thickness profiles of mono- and multilayer MoS_2. (D and E) Tauc plots of the absorption spectra of mono- and multilayer MoS_2, respectively. (F) Schematic diagram of the experimental setup, showing the 2-color excitation and THz wave detection scheme. BS, beam splitter; RM, reflection mirror; BP, birefringent plate; OW, optical wedge; DWP, dual-wavelength waveplate; MRM, metal reflection mirror; PM, 90° off-axis parabolic mirror; WP, Wollaston prism.

3.6 nm; thus, the number of layers of multilayer MoS_2 is estimated to be 5 layers, as shown in Fig. 1C. Additionally, we also measure the ultraviolet–visible absorption spectra of both monolayer and multilayer MoS_2 as shown in Fig. 1D and E. From the absorption spectra, we can determine the direct and indirect optical bandgaps of the monolayer and multilayer MoS_2 to be about 1.82 and 1.35 eV, respectively, using the Tauc plot [54]. Shown in Fig. 1F is the experimental setup. In this experiment, a 1-kHz femtosecond Ti:sapphire amplified laser system that can deliver 6-mJ laser pulses with a pulse duration of ~90 fs and a central wavelength of 800 nm is used. In Fig. 1F, the in-line phase compensator is used to obtain the collinearly polarized 2-color laser fields, and the details of the in-line phase compensator can be found in an early work [34]. The generated THz radiation from the sample is collected and focused by a pair of 90° off-axis parabolic mirrors and then detected by electric-optical sampling with a 1-mm-thick, <110> cut ZnTe crystal.

Results and Discussion

Figure 2A presents the schematic diagram of THz wave generation from MoS_2 material under 2-color light excitation, where the z axis is the direction of light propagation. We measure the THz waveforms (E_p^{THz}) from the mono- and multilayer MoS_2 with the total pump pulse energy of 0.12 mJ and a beam diameter at the sample position of about 2 mm, corresponding to a peak power intensity of ~80 GW/cm^2, as shown in Fig. 2B. The experimental results in Fig. 2B indicate that the THz radiation from monolayer MoS_2 is much lower than that from multilayer MoS_2, probably due to the shorter interaction length for monolayer MoS_2. However, the THz amplitude does not linearly increase with increasing number of layers of MoS_2, since as the layer number increases the MoS_2 sample absorbs more THz radiation and the pump beam. In addition, we estimate the THz electric field to be about 5 and 50 V/cm in mono- and multilayer MoS_2 by comparing with the THz electric field in 2-color laser-induced air plasma, respectively. We further estimate the values of THz electric field from mono- and multilayer MoS_2 to be about 6.25 and 13.89 V/cm for per nanometer scale at normal incidence, respectively. In order to verify that the measured THz waves are indeed generated from MoS_2, we have performed the same experiment using the bare sapphire substrate as the sample and confirmed that there is no detectable THz signal as shown with the black curve in Fig. 2B. The inset in Fig. 2B shows the corresponding spectra obtained by Fourier transform of the THz waveforms in Fig. 2B, indicating a frequency coverage of 0.1 to 3.0 THz, which is essentially limited by the detection bandwidth. To investigate the mechanism of THz wave generation from mono- and multilayer MoS_2, we measure the dependence of the THz peak amplitude on the pump pulse energy, as illustrated in Fig. 2C and D. As the pump pulse energy increases, the THz peak amplitude increases nonlinearly. Therefore, the dependence in Fig. 2C and D indicates that the second-order nonlinear optical process can be excluded since the second-order nonlinear process follows a linear dependence [55]. In Fig. 2C and D, we also observe the decrease in THz peak amplitude for both monolayer and multilayer MoS_2 when the laser pulse energy is higher than 200 μJ due to laser-induced damage.

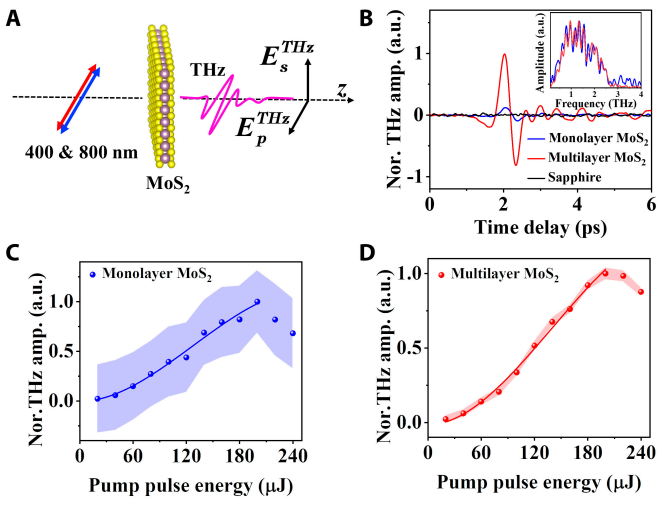

Fig. 2. (A) Schematic diagram of coherent THz wave generation from MoS_2 under collinearly polarized light excitation. (B) THz waveforms and the corresponding Fourier transform spectra of THz waves generated from mono- and multilayer MoS_2. The black curve shows the THz signal from the bare sapphire substrate, indicating no detectable THz radiation. (C and D) Dependence of the THz peak amplitude on the pump pulse energy. The red and blue regions are the error bands of measurement. The red and blue balls are the experimental data, and the red and blue curves are the fitting curves, respectively.

It is worth noting that the third-order nonlinear optical process has been proposed as the mechanism for the THz wave generation from materials in a 2-color light excitation scenario [27,56]. As a third-order nonlinear optical process, coherent injected photocurrent is involved to induce the THz radiation from materials, such as graphene [57] and silicon [37]. QI can be used to clarify the coherent injected photocurrent under 2-color light excitation. The amplitude of the generated THz radiation can be described by the derivative of the photocurrent, $E_{THz} = \partial j/\partial t$. Here, the current density of the coherent injected photocurrent can be expressed as follows when the ω and 2ω pulses are collinearly polarized [21]:

$$\boldsymbol{j}_{\parallel} = 2\boldsymbol{e}_{\boldsymbol{\omega}} i\eta_i^{xxxx} |E_{\omega}|^2 |E_{2\omega}| \sin(\Delta\varphi) \quad (1)$$

where E is the amplitude of the electric field of ω and 2ω pulses, and η is the tensor associated with the third-order susceptibility $\chi^{(3)}$. According to Eq. 1, the photocurrent is related not only to the optical electric fields but also to the relative phase $\Delta\varphi$, making coherent control of the coherent injection current possible. To theoretically fit the experimental data shown in Fig. 2C and D, we further modify Eq. 1 as follows:

$$E_{THz} \propto a\chi^3 I\left(I - bI^2\right) \quad (2)$$

where I is the total pump pulse energy before the barium borate (BBO) crystal, and a and b are constants. The detailed deduction process of the equation was presented in our previous works [36,58]. As shown in the red and blue curves in Fig. 2C and D, Eq. 2 can fit the experimental data well. Thus, we conclude that the mechanism of THz wave generation from MoS_2 materials is a third-order nonlinear optical process.

As mentioned above, Eq. 1 also suggests that the coherent injected photocurrent can be controlled by the relative phase. In the experiment, the relative phase between ω and 2ω pulses can be controlled by changing the insertion depth of one of the optical wedges in the in-line phase compensator due to the different refractive indexes (n) of ω and 2ω pulses in wedges. Then, we can calculate the relative phase between ω and 2ω pulses as follows [34,59]:

$$\Delta\varphi = \omega_{400}\Delta t = \omega_{400}\Delta d\left(n_{400} - n_{800}\right)\tan\left(\theta_w\right)/c \qquad (3)$$

where Δd is the insertion depth of one of the optical wedges in the in-line phase compensator, c is velocity of light, and θ_w = 4° is the wedge angle. Specifically, Eq. 1 indicates that the THz waveforms can be inverted as the relative phase is changed from π/2 to 3π/2. The experimental results in Fig. 3A present the inverted THz waveforms from multilayer MoS_2 when the relative phase is changed by π (from π/2 to 3π/2), agreeing well with Eq. 1. Besides, we also measure the THz peak amplitude as a function of the phase delay by changing the insertion of one of the wedges, as shown in Fig. 3B. The sinusoidal variation of the THz peak amplitude observed in the experimental aligns well with prediction by Eq. 1. Additionally, the phase curve in Fig. 3B exhibits a symmetric distribution centered around the zero axis. Therefore, it suggests that the THz radiation from multilayer MoS_2 is induced only by QI at normal incidence. In addition, we measure the 3D plot of the consecutive THz waveforms from multilayer MoS_2 at different values of the relative phase between the ω and 2ω pulses as shown in Fig. 3C. Figure 3D is the 3D plot of the corresponding Fourier transform spectra. Figure 3C and D simply indicates coherent amplitude control of THz waves from multilayer MoS_2 under 2-color light excitation in the time and frequency domains, respectively. Therefore, the controllable coherent THz radiation (i.e., coherent injected photocurrent) can be realized through the all-optical method in MoS_2.

After we confirm that the THz wave generation from MoS_2 under 2-color laser excitation is attributed to QI, we should consider the band structures of the mono- and multilayer MoS_2. As a typical TMDs material, with the increased number of layers of MoS_2, the band structure of the MoS_2 can be changed from direct to indirect bandgap and the energy of bandgap is decreased [60]. Monolayer MoS_2 has the direct band structure, while multilayer MoS_2 has both indirect and direct band structures. In Fig. 4A, we present the schematic diagram of the direct band structure of the monolayer MoS_2. As shown in Fig. 1D, the bandgap of monolayer MoS_2 is about 1.82 eV, higher than the photon energy of $\hbar\omega$ (1.55 eV) and smaller than that of $2\hbar\omega$ (3.10 eV).

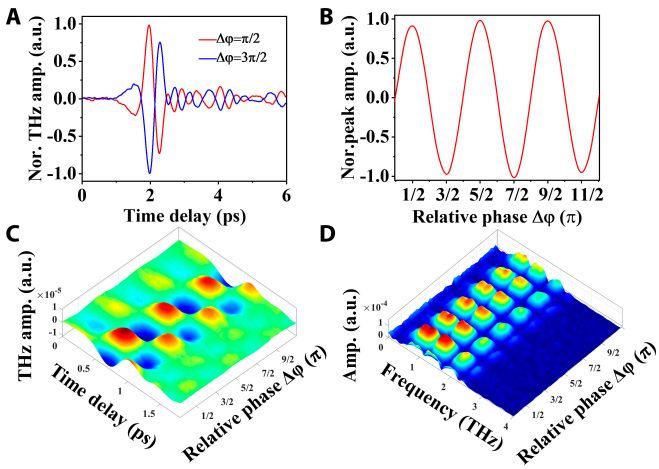

Fig. 3. (A) Reverted THz waveforms from multilayer MoS_2 when the relative phase is changed from π/2 to 3π/2. (B) Dependence of the THz peak amplitude on the relative phase. (C) 3D plot of THz electric field as a function of time delay and relative phase in the time domain. (D) 3D plot of the THz spectra changes in THz amplitude versus the relative phase.

Thus, the electrons in the valence band (VB) can be directly excited to CB through the SPA (400 nm) and TPA (800 nm) transition processes. The SPA of 800-nm photons will be forbidden in monolayer MoS_2. Carrier distribution is asymmetric in CB due to QI under 2-color light excitation as shown in Fig. 4A. This interference effect is a typical QI, and the same effects were observed in traditional direct gap semiconductor materials when $\hbar\omega < E_g < 2\hbar\omega$ [30]. In Fig. 4B, the band structure indicates that multilayer MoS_2 possesses not only the indirect gap (1.35 eV) at Γ point but also the direct gap above 1.8 eV at K point in the Brillouin zone [53]. The direct gap at K point indicates that SPA of 2ω beam can induce vertical inter-band electronic transitions in the Brillouin zone (blue arrows in Fig. 4B). Besides, TPA of ω beam can induce the vertical inter-band electronic transitions near the K point (as enclosed in the blue dashed line in Fig. 4B). These transition pathways of the electrons are also presented in multilayer MoS_2 in previous works [61,62]. Thus, the 2 vertical inter-band electronic transition pathways near the K point of ω and 2ω beams can induce interference, resulting in asymmetric carrier distribution in multilayer MoS_2. Although the direct SPA of ω beam is not allowed in monolayer MoS_2, the indirect SPA of ω beam is unavoidable in the multilayer MoS_2, since the photon energy of the ω beam is higher than the indirect gap of multilayer MoS_2. The electrons near the Γ point are only allowed to be a nonvertical inter-band electronic transitions mediated by the presence of a phonon (as enclosed in the red dashed line in Fig. 4B), while the electrons near the Γ point can also be excited to a higher state in CB [61] by absorbing a 2ω photon and then relax to the minimum CB, emitting a ω photon and liberating phonons (nondegenerated TPA).

In general, most investigations have focused on the photon absorption in direct gap materials for QI, even when the material has indirect bandgap, such as Ge [18]. Therefore, it is necessary to identify QI in multilayer MoS_2 occurring in the direct gap or indirect gap region, or even in both regions. Previous work has demonstrated that the absorption in multilayer MoS_2 is attributed to the direct gap transitions near the K point in the spectral range of 1.3 to 2.4 eV [62]. Thus, the contribution of THz wave generation from the indirect gap may be minor under 2-color light excitation. To further estimate the existence of the contribution from indirect gap region, we give a hypothesis that an additional QI exists in the indirect gap region of multilayer MoS_2. The additional QI is the interference between the transitions from SPA of ω and nondegenerate TPA (2ω absorption and ω emission) near the Γ point. Analogous to the theoretical analysis of graphene [63], the sensitivity to light polarization of the degenerate TPA and nondegenerate TPA is different. Thus, the dependence of THz emission on the relative polarization angle between ω and 2ω will be different when the additional QI exists. Therefore, we can identify the dominant channel of QI in the THz generation process by measuring the dependence of THz emission on the relative polarization angle.

Experimentally, the relative polarization angle (θ) can be controlled by the dual-wavelength waveplate (DWP), which can act as a half-wave plate for the ω beam and a full-wave plate for the 2ω beam as depicted in Fig. 1F. In our experiment, we measure the THz signals (E_p^{THz}) from mono- and multilayer MoS_2 under collinearly (θ = 0°) and cross-linearly (θ = 90°) polarized light excitation, and results are shown in Fig. 4C and D, respectively. For monolayer MoS_2, as shown in Fig. 4C, THz signals with the same polarity are detected under both collinearly and cross-linearly polarized light excitation. Similar experimental

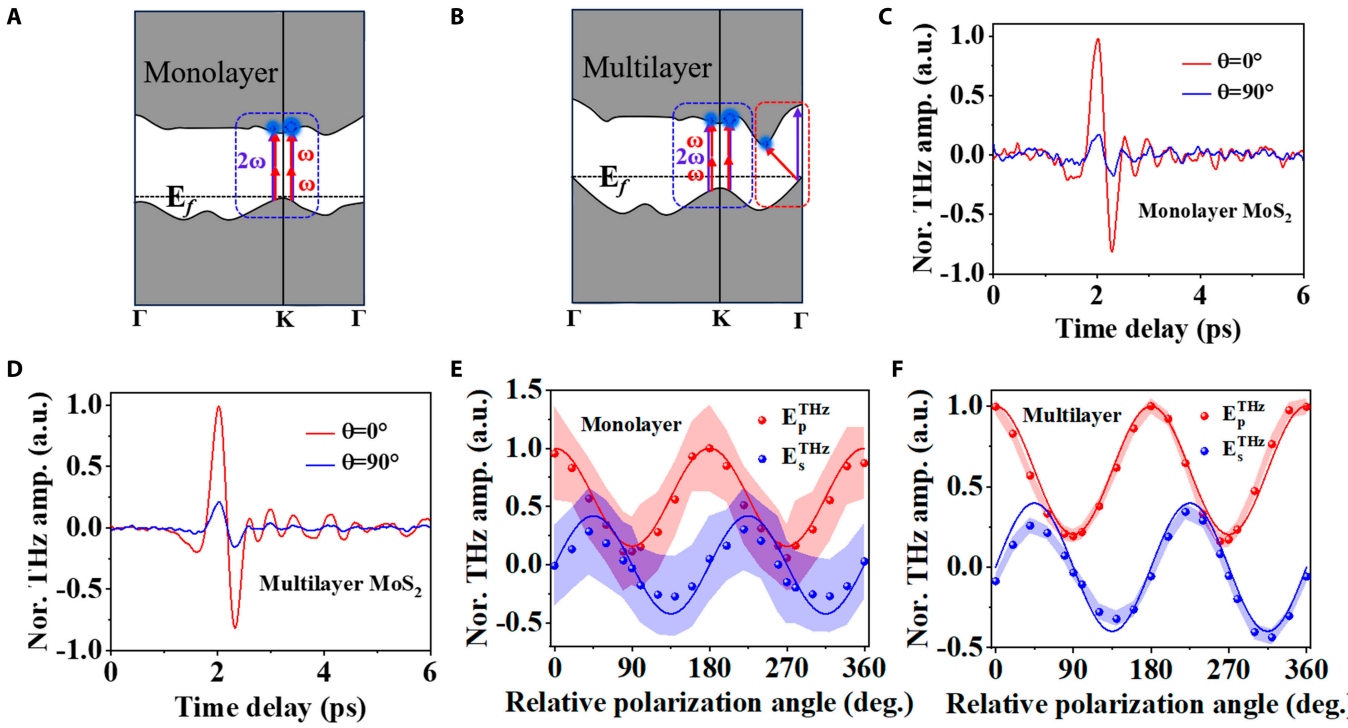

Fig. 4. (A) Schematic diagram of the direct electronic band structure of monolayer MoS_2, and enclosed in the blue dashed line represents the typical QI. (B) Schematic diagram of the indirect electronic band structure of multilayer MoS_2 (as enclosed in the red dashed line). The electron transitions in direct gap region and other transitions in indirect gap region are illustrated in the blue and red dashed lines, respectively. (C and D) THz waveforms from mono- and multilayer MoS_2 when the relative polarization angles (θ) are fixed at 0° and 90°, respectively. (E and F) Dependence of THz peak amplitude on the relative polarization angle for mono- and multilayer MoS_2. The red and blue regions are the error bands of measurement. Red and blue balls are the experimental results, and the red and blue curves are fitting curves.

results are also observed in multilayer MoS_2 as shown in Fig. 4D. Compared with the THz amplitude under collinearly polarized light excitation, the THz amplitude under cross-linearly polarized light excitation is nonnegligible. Similar experimental results under collinearly and cross-linearly polarized light excitation are also demonstrated in GaAs [64] and silicon [37] due to the anisotropy of η. Here, the photocurrent under collinearly polarized light excitation can be expressed by Eq. 1, while the photocurrent under cross-linearly polarized light excitation in MoS_2 can be expressed as follows [65]:

$$\boldsymbol{j}_{\perp} = 2\boldsymbol{e}_{2\omega} i\eta_i^{yxxy} |E_{\omega}|^2 |E_{2\omega}| \sin(\Delta\varphi) \tag{4}$$

From Eqs. 1 and 4, the THz amplitude under collinearly and cross-linearly polarized light excitation is related to η_{xxxx} and η_{yxxy}. The experimental results in Fig. 4C and D are consistent with the anisotropy of the tensor in MoS_2 [66]. Similar experimental results in Fig. 4C and D indicate that the same nonlinear process induces the THz wave generation from mono- and multilayer MoS_2.

To further prove that the same nonlinear process induces the THz wave generation from mono- and multilayer MoS_2, we also measure the dependence of THz peak amplitude on θ as shown in Fig. 4E and F. The experimental results in Fig. 4E and F show similar dependence. In addition, the dependence of E_p^{THz} and E_s^{THz} components on θ can be given from the equation of the coherent injected photocurrent as follows [67]:

$$\begin{pmatrix} E_p^{THz} \\ E_s^{THz} \end{pmatrix} \propto \begin{pmatrix} \cos^2\theta + d\sin^2\theta \\ 1/2(1-d)\sin 2\theta \end{pmatrix} \tag{5}$$

where $d = \eta_{yxxy}/\eta_{xxxx}$ is the disparity parameter. Equation 5 can fit the experimental results in Fig. 4E and F well. The fitting results indicate that the values of d for mono- and multilayer MoS_2 are about 0.16 ± 0.03 and 0.20 ± 0.02, while the R^2 values are about 94% and 98%, respectively. The values of d in mono- and multilayer MoS_2 are essentially the same, and they are roughly consistent with the theoretical calculation of d in monolayer MoS_2 ($d \approx 0.33$) when fundamental photon energy is fixed at 1.55 eV [65]. Therefore, the above discussion of the dependence of THz peak amplitude on θ also indicates that the THz wave generation processes from mono- and multilayer MoS_2 are same. The hypothesis of the additional QI is invalid and confirms that the typical QI dominates THz wave generation from both mono- and multilayer MoS_2 under 2-color light excitation. Thus, QI in multilayer MoS_2 is mainly induced near K point (direct gap region) in the Brillouin zone.

The typical QI induces the THz wave generation from multilayer MoS_2, which is demonstrated in the above discussion. However, previous work of the THz wave generation from MoS_2 under single-color light excitation reveals that OR is the dominant process at oblique incidence [50]. In order to compare the efficiencies of the THz wave generation from multilayer MoS_2 through QI and OR, we study the THz wave generation from multilayer MoS_2 under collinearly polarized light excitation at an incident angle of approximately θ = 45°, as shown in Fig. 5A. In Fig. 5B, we observe the THz wave generation from multilayer MoS_2 under 2-color light excitation when the pump pulse energy is fixed at 120 μJ. The stronger THz radiation can be induced from multilayer MoS_2 than that from monolayer MoS_2 at oblique incidence. Besides, it is hardly to clarify the influence of the efficiency of QI on the film thickness due to

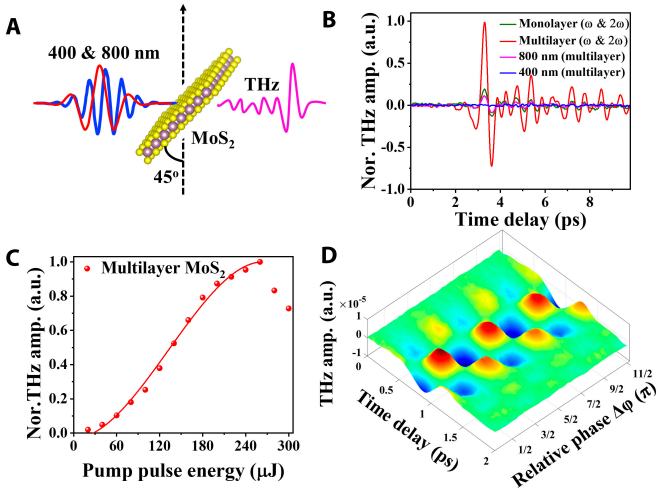

Fig. 5. (A) Schematic diagram of 2-color light excitation scheme at oblique incidence (45°). (B) THz waveforms generated from mono- and multilayer MoS_2 under 2-color light excitation and THz waveforms generated from multilayer MoS_2 under single-color light excitation when we fix the oblique incidence at 45°. (C) Dependence of the THz peak amplitude on the pump pulse energy. Red balls are experimental data, and red curve is the fitting curve. (D) 3D plot of the coherent THz amplitude as a function of time delay and relative phase in the time domain in multilayer MoS_2 under 2-color light excitation at oblique incidence.

the complex nonlinear processes at oblique incidence [27]. The experimental results in Fig. 5B also indicate that THz wave generation can be detected at oblique incidence under single-color (800 nm) light excitation and no THz response can be detected under 400-nm light excitation. The individual pump pulse energies of ω and 2ω under single-color light excitation are equal to those of laser pulses that make up the 2-color laser fields, respectively. Furthermore, in Fig. 5B, it should be noted that THz amplitude under 2-color light excitation is approximately 10 times of that under single-color light excitation in multilayer MoS_2. Thus, THz wave generation efficiency through QI is higher than that through OR in multilayer MoS_2, which agrees with the previous conclusion on the THz wave generation from ZnTe crystal through QI and OR [35]. To confirm the mechanism of the THz wave generation in the case of Fig. 5A, we measure the dependence of THz peak amplitude on the pump pulse energy, and the experimental results can be fitted well by Eq. 2 as shown in Fig. 5C, verifying that the generation process is attributed to the third-order nonlinearity induced by QI. Besides, we also measure the 3D plot of the electric field of the THz radiation from multilayer MoS_2 as a function of the time delay for the THz waveform scan and the relative phase between the ω and 2ω pulses, and results are shown in Fig. 5D. The experimental results in Fig. 5D show that the coherent THz wave generation can be controlled by the relative phase and the experimental results exhibit a symmetric distribution centered around the zero axis. Therefore, QI can still be the dominant process in the THz wave generation.

Conclusion

In summary, we employ 2-color light excitation to study the coherent injected photocurrent by detecting the generated THz waves from mono- and multilayer MoS_2 materials with thickness at nanometer scale. The dependence of the THz amplitude on the pump pulse energy indicates that THz wave generation from MoS_2 can be attributed to a third-order nonlinear process. Further experimental results on coherent control of THz amplitude by changing the relative phase between the ω and 2ω pulses prove that QI induces the THz wave generation from both mono- and multilayer MoS_2. Besides, we present experimental evidences of the nonnegligible component of the coherent injected photocurrent under cross-polarized light excitation. We verify that the typical QI in direct gap region induces the coherent injected photocurrent in both mono- and multilayer MoS_2 by performing experiments on the dependence of THz amplitude on the relative polarization angle. In addition, the experimental results under 2-color and single-color light excitation at oblique incidence in multilayer MoS_2 indicate that QI is the dominant process and shows more efficiency than OR for THz wave generation in MoS_2 under oblique laser excitation. This work enriches our understanding of the generation and control of coherent injected photocurrent using 2-color light excitation in MoS_2 materials and provides deeper insight into the process of QI in materials with an indirect gap.

Acknowledgments

Funding: This work is supported by the National Science Foundation of China (NSFC) (nos. 62375199, 62075157, and 62235013), Tianjin Municipal Fund for Distinguished Young Scholars (grant no. 20JCJQJC00190), and Key Fund of Shenzhen Natural Science Foundation (grant no. JCYJ20200109150212515).
Author contributions: Y.H. carried out the experiments, collected and analyzed the data, and composed the first draft. Y.C. designed the experiment setup and developed the numerical study. X.L. and C.D. helped the sample characterization and drawn some figures. Z.T. and J.D. developed the idea, initiated the research, and supervised the whole project. All authors contributed to the final version of the manuscript.
Competing interests: The authors declare that they have no competing interests.

Data Availability

The data reported in this article are freely available upon request to the authors.

References

1. Ferguson B, Zhang X-C. Materials for terahertz science and technology. *Nat Mater*. 2002;1(1):26–33.
2. Fülöp JA, Tzortzakis S, Kampfrath T. Laser-driven strong-field terahertz sources. *Adv Opt Mater*. 2020;8(3):1900681.
3. Zhao Y, Yang Y, Sun H-B. Nonlinear meta-optics towards applications. *PhotoniX*. 2021;2:3.
4. Stantchev RI, Yu X, Blu T, Pickwell-MacPherson E. Real-time terahertz imaging with a single-pixel detector. *Nat Commun*. 2020;11(1):2535.
5. Lee G, Lee J, Park QH, Seo M. Frontiers in terahertz imaging applications beyond absorption cross-section and diffraction limits. *ACS Photonics*. 2022;9(5):1500–1512.
6. Yang Z, Tang D, Hu J, Tang M, Zhang M, Cui H-L, Wang L, Chang C, Fan C, Li J, et al. Near-field nanoscopic terahertz imaging of single proteins. *Small*. 2021;17(3):2005814.
7. Jepsen PU, Cooke DG, Koch M. Terahertz spectroscopy and imaging—Modern techniques and applications. *Laser Photonics Rev*. 2011;5(1):124–166.

8. Peng Y, Shi C, Zhu Y, Gu M, Zhuang S. Terahertz spectroscopy in biomedical field: A review on signal-to-noise ratio improvement. *PhotoniX*. 2020;1:12.
9. Mittendorff M, Winnerl S, Murphy TE. 2D THz optoelectronics. *Adv Opt Mater*. 2021;9(3):2001500.
10. Qiu Q, Huang Z. Photodetectors of 2D materials from ultraviolet to terahertz waves. *Adv Mater*. 2021;33(15):2008126.
11. Rice A, Jin Y, Ma XF, Zhang XC, Bliss D, Larkin J, Alexander M. Terahertz optical rectification from ⟨110⟩ zinc-blende crystals. *Appl Phys Lett*. 1994;11(64):1324.
12. Carletti L, McDonnell C, Arregui Leon U, Rocco D, Finazzi M, Toma A, Ellenbogen T, Della Valle G, Celebrano M, De Angelis C. Nonlinear THz generation through optical rectification enhanced by phonon–polaritons in lithium niobate thin films. *ACS Photonics*. 2023;10(9):3419–3425.
13. Maysonnave J, Huppert S, Wang F, Maero S, Berger C, de Heer W, Norris TB, De Vaulchier LA, Dhillon S, Tignon J, et al. Terahertz generation by dynamical photon drag effect in graphene excited by femtosecond optical pulses. *Nano Lett*. 2014;14(10):5797–5802.
14. Zhang L, Zhang D, Hu F, Xu X, Zhao Q, Sun X, Wu H, Lü Z, Wang X, Zhao Z. Generation and control of ultrafast circular photon drag current in multilayer $PtSe_2$ revealed via terahertz emission. *Adv Opt Mater*. 2023;11(2):2201881.
15. Tong M, Hu Y, He W, Yu X-L, Hu S. Ultraefficient terahertz emission mediated by shift-current photovoltaic effect in layered gallium telluride. *ACS Nano*. 2021;15(11):17565–17572.
16. Obraztsov PA, Lyashenko D, Chizhov PA, Konishi K, Nemoto N, Kuwata-Gonokami M, Welch E, Obraztsov AN, Zakhidov A. Ultrafast zero-bias photocurrent and terahertz emission in hybrid perovskites. *Commun Phys*. 2018;1:14.
17. Pettine J, Padmanabhan P, Sirica N, Prasankumar RP, Taylor AJ, Chen HT. Ultrafast terahertz emission from emerging symmetry-broken materials. *Light Sci Appl*. 2023;12(1):133.
18. Spasenović M, Betz M, Costa L, van Driel HM. All-optical coherent control of electrical currents in centrosymmetric semiconductors. *Phys Rev B*. 2008;77(8):Article 085201.
19. Fraser JM, Shkrebtii AI, Sipe JE, Van Driel HM. Quantum interference in electron-hole generation in noncentrosymmetric semiconductors. *Phys Rev Lett*. 1999;83(20):4192–4195.
20. Haché A, Kostoulas Y, Atanasov R, Hughes JLP, Sipe JE, Driel HMV. Observation of coherently controlled photocurrent in unbiased, bulk GaAs. *Phys Rev Lett*. 1997;78(2):306–309.
21. Côté D, Fraser JM, Decamp M, Bucksbaum PH, Van Driel HM. THz emission from coherently controlled photocurrents in GaAs. *Appl Phys Lett*. 1999;75:3959–3961.
22. Cook DJ, Hochstrasser RM. Intense terahertz pulses by four-wave rectification in air. *Opt Lett*. 2000;25(16):1210–1212.
23. Jin Q, Dai J. Terahertz wave emission from a liquid water film under the excitation of asymmetric optical fields. *Appl Phys Lett*. 2018;113:Article 261101.
24. Yuxuan C, Yuhang H, Liyuan L, Zhen T, Xi-Cheng Z, Jianming D. Plasma-based terahertz wave photonics in gas and liquid phases. *Photonics Insights*. 2023;2:R06.
25. Sun D, Divin C, Rioux J, Sipe JE, Berger C, de Heer WA, First PN, Norris TB. Coherent control of ballistic photocurrents in multilayer epitaxial graphene using quantum interference. *Nano Lett*. 2010;10(4):1293–1296.
26. Heide C, Eckstein T, Boolakee T, Gerner C, Weber HB, Franco I, Hommelhoff P. Electronic coherence and coherent dephasing in the optical control of electrons in graphene. *Nano Lett*. 2021;21(22):9403–9409.
27. Totero Gongora JS, Peters L, Tunesi J, Cecconi V, Clerici M, Pasquazi A, Peccianti M. All-optical two-color terahertz emission from quasi-2D nonlinear surfaces. *Phys Rev Lett*. 2020;125(26):Article 263901.
28. Bhat R, Sipe J. Optically injected spin currents in semiconductors. *Phys Rev Lett*. 2000;85(25):5432–5435.
29. Ruzicka BA, Zhao H. Optical studies of ballistic currents in semiconductors. *J Opt Soc Am B*. 2012;29(2):A43–A54.
30. Zhao H, Loren EJ, Smirl AL, van Driel HM. Dynamics of charge currents ballistically injected in GaAs by quantum interference. *J Appl Phys*. 2008;103:201.
31. Bas DA, Vargas-Velez K, Babakiray S, Johnson TA, Borisov P, Stanescu TD, Lederman D, Bristow AD. Coherent control of injection currents in high-quality films of Bi_2Se_3. *Appl Phys Lett*. 2015;106:Article 041109.
32. Christian S, Jean-Michel M, Markus B, Arthur L. All-optical coherently controlled terahertz ac charge currents from excitons in semiconductors. *Phys Rev B*. 2009;79(4):45208.
33. Zhihui Lü DZ, Zhou Z, Sun L, Zhao Z, Yuan J. Coherently controlled terahertz source for a time domain spectroscopy system via injection current in bulk ZnSe. *Appl Opt*. 2012;51(5):676–679.
34. Dai JM, Karpowicz N, Zhang XC. Coherent polarization control of terahertz waves generated from two-color laser-induced gas plasma. *Phys Rev Lett*. 2009;103(2): Article 023001.
35. Peters L, Totero Gongora JS, Cecconi V, Olivieri L, Tunesi J, Pasquazi A, Peccianti M. Concurrent terahertz generation via quantum interference in a quadratic media. *Adv Opt Mater*. 2023;11(15):2202578.
36. He Y, Chen Y, Zhao J, Tian Z, Dai J. Coherent terahertz radiation from indium tin oxide film via third-order optical nonlinearity. *Appl Phys Lett*. 2023;122(4):Article 041106.
37. Costa L, Betz M, Spasenović M, Bristow AD, van Driel HM. All-optical injection of ballistic electrical currents in unbiased silicon. *Nat Phys*. 2007;3:632–635.
38. Autere A, Jussila H, Dai Y, Wang Y, Lipsanen H, Sun Z. Nonlinear optics with 2D layered materials. *Adv Mater*. 2018;30(24):1705963.
39. Chhowalla M, Liu Z, Zhang H. Two-dimensional transition metal dichalcogenide (TMD) nanosheets. *Chem Soc Rev*. 2015;44(9):2584–2586.
40. Tongay S, Zhou J, Ataca C, Lo K, Matthews TS, Li J, Grossman JC, Wu J. Thermally driven crossover from indirect toward direct bandgap in 2D semiconductors: $MoSe_2$ versus MoS_2. *Nano Lett*. 2012;12(11):5576–5580.
41. Steinhoff A, Kim JH, Jahnke F, Rösner M, Kim DS, Lee C, Han GH, Jeong MS, Wehling TO, Gies C. Efficient excitonic photoluminescence in direct and indirect band gap monolayer MoS_2. *Nano Lett*. 2015;15(10):6841–6847.
42. Li X, Zhu H. Two-dimensional MoS_2: Properties, preparation, and applications. *J Mater*. 2015;1(1):33–44.
43. Yin Z, Li H, Li H, Jiang L, Shi Y, Sun Y, Lu G, Zhang Q, Chen X, Zhang H. Single-layer MoS_2 phototransistors. *ACS Nano*. 2012;6(1):74–80.
44. Kufer D, Konstantatos G. Highly sensitive, encapsulated MoS_2 photodetector with gate controllable gain and speed. *Nano Lett*. 2015;15(11):7307–7313.
45. Xie Y, Zhang B, Wang S, Wang D, Wang A, Wang Z, Yu H, Zhang H, Chen Y, Zhao M, et al. Ultrabroadband MoS_2

photodetector with spectral response from 445 to 2717 nm. *Adv Mater*. 2017;29(17):1605972.
46. Tsai M-L, Su S-H, Chang J-K, Tsai D-S, Chen C-H, Wu C-I, Li L-J, Chen L-J, He J-H. Monolayer MoS_2 heterojunction solar cells. *ACS Nano*. 2014;8(8):8317–8322.
47. Zhang S, Dong N, McEvoy N, O'Brien M, Winters S, Berner NC, Yim C, Li Y, Zhang X, Chen Z, et al. Direct observation of degenerate two-photon absorption and its saturation in WS_2 and MoS_2 monolayer and few-layer films. *ACS Nano*. 2015;9(7):7142–7150.
48. Lee J, Wang Z, He K, Yang R, Shan J, Feng PX-L. Electrically tunable single- and few-layer MoS_2 nanoelectromechanical systems with broad dynamic range. *Sci Adv*. 2018;4(3):eaao6653.
49. Huang Y, Zhu L, Zhao Q, Guo Y, Ren Z, Bai J, Xu X. Surface optical rectification from layered MoS_2 crystal by THz time-domain surface emission spectroscopy. *ACS Appl Mater Interfaces*. 2017;9(5):4956–4965.
50. Huang Y, Zhu L, Yao Z, Zhang L, He C, Zhao Q, Bai J, Xu X. Terahertz surface emission from layered MoS_2 crystal: Competition between surface optical rectification and surface photocurrent surge. *J Phys Chem C*. 2017;122(1):481–488.
51. Li H, Zhang Q, Yap CCR, Tay BK, Edwin THT, Olivier A, Baillargeat D. From bulk to monolayer MoS_2: Evolution of Raman scattering. *Adv Funct Mater*. 2012;22(7):1385–1390.
52. Watson GH Jr, Daniels WB, Wang CS. Measurements of Raman intensities and pressure dependence of phonon frequencies in sapphire. *J Appl Phys*. 1981;52:956–958.
53. Splendiani A, Sun L, Zhang Y, Li T, Kim J, Chim C-Y, Galli G, Wang F. Emerging photoluminescence in monolayer MoS_2. *Nano Lett*. 2010;10(4):1271–1275.
54. Makuła P, Pacia M, Macyk W. How to correctly determine the band gap energy of modified semiconductor photocatalysts based on UV–vis spectra. *J Phys Chem Lett*. 2018;9(23):6814–6817.
55. Huang Y, Yao Z, He C, Zhu L, Zhang L, Bai J, Xu X. Terahertz surface and interface emission spectroscopy for advanced materials. *J Phys Condens Matter*. 2019;31(15):Article 153001.
56. He Y, Chen Y, Lu C, Zhang Y, Tian Z, Xu X, Dai J. Coherent injection photocurrent in bismuth sulfide film induced by one-plus-two photon absorption quantum interference. *Opt Lett*. 2022;47(5):1206–1209.
57. Sun D, Rioux J, Sipe JE, Zou Y, Mihnev MT, Berger C, de Heer WA, First PN, Norris TB. Evidence for interlayer electronic coupling in multilayer epitaxial graphene from polarization-dependent coherently controlled photocurrent generation. *Phys Rev B*. 2012;85(16):Article 165427.
58. Dai J, Xie X, Zhang X-C. Terahertz wave amplification in gases with the excitation of femtosecond laser pulses. *Appl Phys Lett*. 2007;91:Article 211102.
59. Xie X, Dai J, Zhang X-C. Coherent control of THz wave generation in ambient air. *Phys Rev Lett*. 2006;96(7):Article 075005.
60. Ellis JK, Lucero MJ, Scuseria GE. The indirect to direct band gap transition in multilayered MoS_2 as predicted by screened hybrid density functional theory. *Appl Phys Lett*. 2011;99:Article 211102.
61. Hu J, Xiang Y, Ferrari BM, Scalise E, Vanacore GM. Indirect exciton-phonon dynamics in MoS_2 revealed by ultrafast electron diffraction. *Adv Funct Mater*. 2023;33(19):2206395.
62. Mak KF, Lee C, Hone J, Shan J, Heinz TF. Atomically thin MoS_2: A new direct-gap semiconductor. *Phys Rev Lett*. 2010;105:Article 136805.
63. Rioux J, Sipe JE, Burkard G. Interference of stimulated electronic Raman scattering and linear absorption in coherent control. *Phys Rev B*. 2014;90(11):Article 115424.
64. Atanasov R, Haché A, Hughes JLP, Van Driel HM, Sipe JE. Coherent control of photocurrent generation in bulk semiconductors. *Phys Rev Lett*. 1996;76(10):1703–1706.
65. Muniz RA, Sipe JE. All-optical injection of charge, spin, and valley currents in monolayer transition-metal dichalcogenides. *Phys Rev B*. 2015;91(8):Article 085404.
66. Liu F, Zhao X, Yan X-Q, Xin X, Liu Z-B, Tian J-G. Measuring third-order susceptibility tensor elements of monolayer MoS_2 using the optical Kerr effect method. *Appl Phys Lett*. 2018;113(5):Article 051901.
67. Newson RW, Green AA, Hersam MC, van Driel HM. Coherent injection and control of ballistic charge currents in single-walled carbon nanotubes and graphite. *Phys Rev B*. 2011;83(11):Article 115421.